AGU PUBLICATIONS

Geophysical Research Letters

RESEARCH LETTER
10.1002/2017GL072908

Key Points:
- The El Niño-Southern Oscillation tightly controls interannual variations in the heating rate of the tropical atmosphere ($r > 0.9$)
- A physically based simple model is constructed to reproduce the history of global mean surface temperature since the 1880s
- The global warming hiatus since 2000 resulted from weak El Niño activity and ended when warm conditions set in the tropics in 2014–2016

Supporting Information:
- Supporting Information S1

Correspondence to:
S. Hu,
shineng.hu@yale.edu

Citation:
Hu, S., and A. V. Fedorov (2017), The extreme El Niño of 2015–2016 and the end of global warming hiatus, *Geophys. Res. Lett.*, *44*, 3816–3824, doi:10.1002/2017GL072908.

Received 1 FEB 2017
Accepted 30 MAR 2017
Accepted article online 3 APR 2017
Published online 22 APR 2017

The extreme El Niño of 2015–2016 and the end of global warming hiatus

Shineng Hu[1] and **Alexey V. Fedorov**[1]

[1]Department of Geology and Geophysics, Yale University, New Haven, Connecticut, USA

Abstract Slower rates of increase in global mean surface temperature (GMST) after 2000, dubbed "global warming hiatus," recently gave way to a rapid temperature rise. This rise coincided with persistent warm conditions in the equatorial Pacific between March 2014 and May 2016, which peaked as the 2015 extreme El Niño. Here we show that the El Niño–Southern Oscillation (ENSO) tightly controls interannual variations in atmospheric heating rate in the tropics ($r > 0.9$), allowing us to construct a simple, physically based model of GMST variations that incorporates greenhouse gas emissions, ENSO forcing, and stratospheric sulfate aerosols produced by volcanoes. The model closely reproduces GMST changes since 1880, including the global warming hiatus and the subsequent temperature rise. Our results confirm that weak El Niño activity, rather than volcanic eruptions, was the cause of the hiatus, while the rapid temperature rise is due to atmospheric heat release during 2014–2016 El Niño conditions concurrent with the continuing global warming trend.

1. Introduction

During 2014–2016, the tropical Pacific experienced prolonged warm conditions that included a weak El Niño in 2014 and an extreme El Niño in 2015–2016, as reflected in positive sea surface temperature (SST) anomalies and higher-than-normal sea level along the equator (Figures 1a and 1b). Recent studies suggest that the development of both events was strongly shaped by the interplay between westerly and easterly wind bursts that occurred over the tropical Pacific [*Menkes et al.*, 2014; *McPhaden*, 2015; *Levine and McPhaden*, 2016; *Hu and Fedorov*, 2016, 2017]. For instance, the 2014 El Niño, while rapidly developing during the first half of the year, was stalled by year-end, presumably impacted by a strong midsummer easterly wind burst [*Hu and Fedorov*, 2016]. As this weak event did not exceed a formal threshold, it is sometimes referred to as a failed El Niño. In contrast, the 2015 El Niño, aided by a strong sequence of westerly wind bursts, reached as large magnitudes as the previous extreme event of 1997 with SST anomalies exceeding 4°C (Figures 1d and 1e). In the end, the total duration of the recent warm conditions in the tropical Pacific far exceeded that of 1997–1998.

At the same time, global mean surface temperature (GMST) has been rapidly increasing, making 2014, 2015, and 2016 the three consecutive warmest years of the instrumental record so far [*NASA News*, 2017]. Thus, this temperature rise effectively ended the global warming "hiatus" implied by the slower rates of GMST increase since the year 2000 [e.g., *Schmidt et al.*, 2014; *Fyfe et al.*, 2016]. Even though a number of physical mechanisms were proposed to explain the hiatus, including but not limited to eastern Pacific cooling, Walker Cell strengthening, enhanced ocean heat uptake, and changes in stratospheric water vapor and aerosols, its exact causes have been hotly debated [e.g., *Lyman et al.*, 2010; *Solomon et al.*, 2010, 2011; *Kaufmann et al.*, 2011; *Levitus et al.*, 2012; *Kosaka and Xie*, 2013; *Huber and Knutti*, 2014; *England et al.*, 2014; *Santer et al.*, 2014; *Schmidt et al.*, 2014; *Watanabe et al.*, 2014; *Dai et al.*, 2015; *Xie et al.*, 2015; *Liu et al.*, 2016; *Zhang*, 2016; *Dong and McPhaden*, 2017]; some argue that the hiatus itself depends on the data sets and the methods of analysis used [*Karl et al.*, 2015].

It is well recognized that the El Niño–Southern Oscillation (ENSO) dominates interannual climate variability, contributing to interannual variations of GMST [e.g., *Philander*, 1990]. This connection can be used to subtract the ENSO signal from GMST to reveal long-term greenhouse warming trends [*Thompson et al.*, 2009; *Santer et al.*, 2014]. However, correlations between GMST and ENSO indices are relatively low even when time lags are taken into account, typically in the range of 0.3–0.5 [*Trenberth et al.*, 2002; *Thompson et al.*, 2009]. For example, the correlation between July–June annual-mean GMST and equatorial SST anomalies averaged within 5°S–5°N, 160°E–90°W (called T_{NINO} hereafter; see section 2) is only about 0.5 (Figure S1 in the

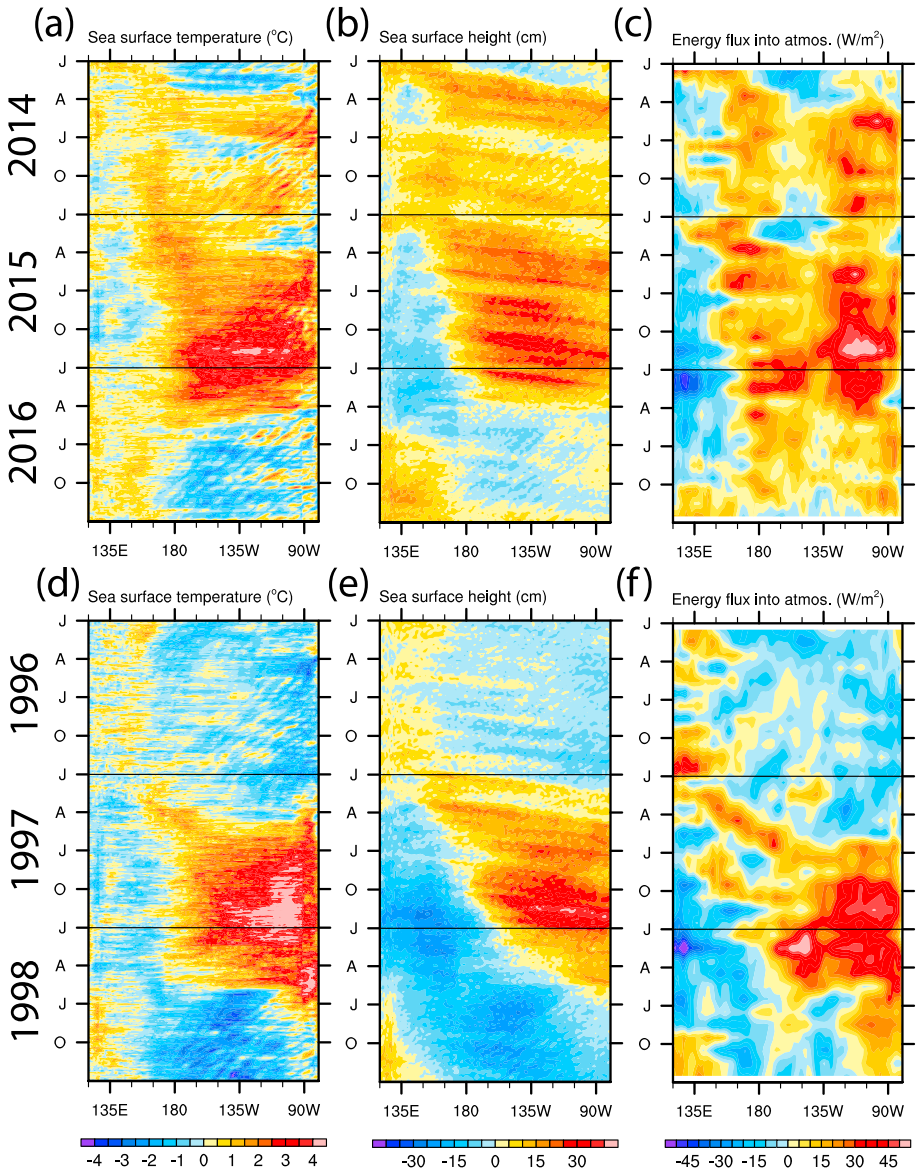

Figure 1. Hovmoller diagrams for equatorial anomalies in (a and d) SST, (b and e) sea level height, and (c and f) atmospheric vertical energy convergence for two periods: 2014–2016 and 1996–1998. Note the extreme El Niño events in 2015 and 1997. SST and sea level anomalies are with respect to a 1995–2005 climatological mean, averaged within the equatorial band (2°S–2°N). Vertical energy convergence (positive into the atmosphere) includes both turbulent heat fluxes at the ocean surface and radiative fluxes at the ocean surface and the top of the atmosphere; it is computed with respect to a 1982–2011 climatological mean and is averaged within the tropical band (15°S–15°N). Note the prolonged warm conditions and persistent atmospheric heating during 2014–2016.

supporting information). This number reduces to 0.4 or even 0.3 if the standard Niño3.4 index is used and/or the annual mean is defined for the January–December interval.

In this study, we revisit the connection between ENSO and GMST and build a simple, physically based model aimed to reproduce historical global temperature variations since the 1880s. The structure of the paper is as follows. Data sets and methods are described in section 2. The ENSO-GMST connection is discussed in section 3, with a particular focus on ENSO-related heating of the tropical atmosphere. In section 4, we construct the simple model and discuss the model performance. In section 5, we present the results from the simple model with a particular focus on the recent hiatus and the subsequent rapid temperature rise. A brief summary and potential applications of this model are presented in the last section.

2. Data and Methods

To show the spatiotemporal patterns of the El Niño events in Figures 1a and 1b, we employ high-resolution satellite observations. Specifically, for tropical SST maps, we use NOAA Optimum Interpolation SST V2 product [*Reynolds et al*., 2007], provided by NOAA Earth System Research Laboratory (ESRL) Physical Sciences Division (http://www.esrl.noaa.gov/psd/data). For sea level, we use Archiving, Validation, and Interpretation of Satellite Oceanographic data (AVISO) absolute dynamic topography product that was produced by Segment Sol multi-missions dALTimetrie, d'orbitographie et de localisation précise/Data Unification and Altimeter Combination System (SSALTO/DUACS) and distributed by AVISO, with support from Centre National d'Etudes Spatiales (http://www.aviso.altimetry.fr/duacs/). For the energy flux analysis, we use surface and radiative fluxes from the ERA-Interim reanalysis (http://www.ecmwf.int/en/research/climate-reanalysis/era-interim). For statistical analyses in Figure 2, energy fluxes are detrended as the magnitudes and signs of the trends show large variations across different data sets [*Liang and Yu*, 2016].

For global temperatures spanning the period of 1880–2016, we use Goddard Institute for Space Studies (GISS) Surface Temperature Analysis with a 1200 km smoothing to calculate the GMST [*Hansen et al*., 2010; *Goddard Institute for Space Studies Surface Temperature Analysis Team*, 2017]. To evaluate ENSO variations, we use Extended Reconstructed Sea Surface Temperature v4 SST product. For CO_2 concentrations, we use Mauna Loa in situ measurements downloaded from NOAA Earth System Research Laboratory (ESRL) website (www.esrl.noaa.gov/gmd/ccgg/trends/) available after 1959, combined with ice core reconstructions from Law Dome DE08 and DE08-2 (http://cdiac.ornl.gov/ftp/trends/co2/lawdome.smoothed.yr20) before that. The two data sets are in close agreement during the overlapping period of 1959–1978 (Figure S4). To account for volcanic eruptions, we employ a stratospheric aerosol optical depth data set from NASA GISS [*Sato et al*., 1993].

To capture different types of El Niño flavor, i.e., Central Pacific and Eastern Pacific events [e.g., *Kao and Yu*, 2009; *Kug et al*., 2009; *Hu et al*., 2014; *Fedorov et al*., 2015; *Capotondi et al*., 2015], we define an ENSO index, T_{NINO}, by averaging SST anomalies within a large equatorial Pacific domain between 160°E–90°W and 5°S–5°N. This index incorporates both the Niño3 and Niño4 regions (the black dashed box in Figure 2a).

All annual means in this study are defined for the July–June interval, rather than the calendar January–December, to capture the ENSO seasonal phase-locking as El Niño and La Niña typically peak in December [e.g., *Neelin et al*., 2000].

To evaluate atmospheric heating rates due to ENSO, we compute net anomalous vertical energy convergence over a tropical Pacific region confined between 160°E–90°W and 15°S–15°N (the black dashed box in Figure 2c). This energy (or heat) convergence, hereafter denoted as Q_{TropPac}, accounts for turbulent sensible and latent heat fluxes at the ocean surface and net shortwave and longwave radiative fluxes at the ocean surface and at the top of the atmosphere (positive into the atmosphere).

3. The Connection Between ENSO and GMST Revisited

During El Niño events, changes in the tropical Pacific modify turbulent heat fluxes at the ocean-atmosphere interface, leading to anomalous vertical energy convergence into the tropical atmosphere, as was observed during the 2015 and 1997 extreme events (Figures 1c and 1f). A composite analysis for all historical El Niño events since 1979 confirms that positive atmospheric heating anomalies develop over most of the tropical Pacific (Figures 2a and 2c), dominated by surface latent heat fluxes (Figure S2). Negative anomalies occur over the Maritime continent, resulting mainly from a longwave radiative flux increase due to the eastward migration of convective clouds, but these anomalies are relatively weak and largely compensated by adjacent positive anomalies in the central Pacific (Figure 2c).

Net atmospheric heating anomalies Q_{TropPac}, when averaged within the tropical Pacific domain, highly correlate with the ENSO index T_{NINO} (Figures 2b and 2d). For annual-mean values, this correlation can be as high as 0.91 (Figure 2e). Even greater correlations are found in general circulation models such as the Community Earth System Model (CESM) ($r = 0.96$), with the model regression slope between the two variables similar to that in the reanalysis (Figure 2f). For this comparison we used a preindustrial simulation of version 1.0.6 of the model [*Deser et al*., 2012].

Point-correlation maps relating local vertical energy convergence in the Pacific and T_{NINO} closely resemble the energy flux composites, which further validates this relationship (Figure S3). These results confirm that

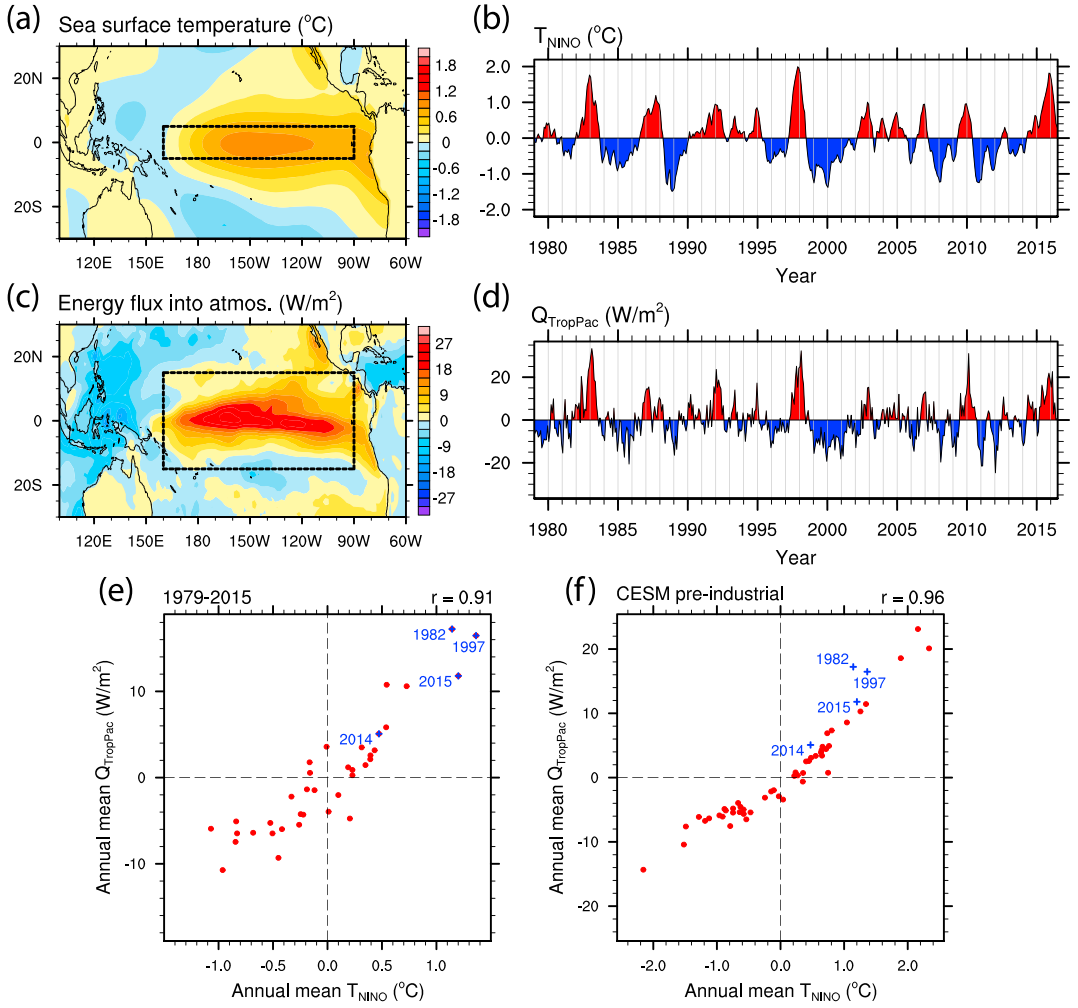

Figure 2. (a and c) Composites of annual-mean anomalies in SST and atmospheric vertical energy convergence for El Niño years during 1979–2015. (b and d) The corresponding temporal variations in T_{NINO} and energy flux convergence $Q_{TropPac}$ averaged within the boxes shown in Figures 2a and 2c, respectively. (e and f) Annual-mean anomalies in the vertical energy flux convergence $Q_{TropPac}$ versus T_{NINO} for the (left) ERA-interim 1979–2015 reanalysis and a (right) CESM preindustrial simulation. The tight correlation between the two variables is found in both the reanalysis and the CESM simulation. $Q_{TropPac}$ and T_{NINO} are defined in section 2. Energy convergence is detrended and considered positive into the atmosphere. Annual means are computed for July–June intervals.

ENSO very tightly regulates vertical energy convergence and hence heating rates of the tropical atmosphere, which must affect the rate of change of GMST.

During the prolonged warm conditions of 2014–2016 the heating of the tropical atmosphere persisted for over 2 years (Figure 1c), resulting in a total atmospheric heat release greater than that during the 1997 El Niño (Figure 1f). As we will show next, this large amount of heat release was a dominant factor that contributed to the ending of the global warming hiatus.

4. A Simple Model for GMST

Motivated by these results, we now construct a simple model for GMST variations with the goal of reproducing global temperature history during the instrumental era and with a particular focus on the recent hiatus and the subsequent rapid temperature rise. The model incorporates the main factors affecting GMST and is based on a first-order differential equation describing the rate of change of annual-mean GMST:

$$\frac{dT_g}{dt} = -\frac{T_g}{\tau} + a \cdot \log\left(CO_2/CO_{2,\mathrm{ref}}\right) + b \cdot T_{\mathrm{NINO}} + c \cdot \mathrm{SAOD} + d, \quad (1)$$

where T_g stands for annual-mean GMST. This equation allows us to predict GMST variations, if the initial GMST value is known. The model assumes a finite effective heat capacity of the system that may change for different processes; these differences are incorporated in the model's coefficients. The computations require data on atmospheric CO_2 concentration, anomalous vertical atmospheric energy (heat) convergence due to ENSO, and radiative effects of volcanic eruptions. Other well-mixed greenhouse gases and anthropogenic aerosols are not included—it is assumed that their radiative effects largely compensate each other [*Myhre et al*., 2013] and the residual can be incorporated in the CO_2 forcing. Nor does the model include insolation changes due to solar cycles, which are an order of magnitude weaker than the ENSO related heating.

The particular terms on the right-hand side of equation (1) describe (i) linear damping with an *e*-folding time scale τ, (ii) longwave radiative forcing due to greenhouse gases (mainly carbon dioxide), (iii) atmospheric heating anomalies associated with ENSO (positive into the atmosphere and assumed proportional to T_{NINO}), (iv) shortwave scattering by stratospheric sulfate aerosols induced by volcanic eruptions, and (v) a constant term, respectively. The relaxation time scale τ is set to 2 years. We use a natural logarithm of CO_2 concentration since it correlates better with the radiative forcing. T_{NINO} refers to the ENSO index defined in section 2 with its long-term warming trend removed; no filtering has been applied, and thus, the ENSO forcing contains a broad range of time scales from interannual to interdecadal. SAOD stands for stratospheric aerosol optical depth. The last constant term is related to how the reference CO_2 concentration is chosen; here we set $CO_{2,ref}$ = 320 ppm. Individual forcings are shown in Figure S4. Model integrations start from the initial condition of 1880; 1 year is used as the time step.

Coefficients *a*, *b*, *c*, and *d* are found by minimizing the root-mean-square (RMS) error of the model results relative to the observed GMST record for 1880–2016 with the mean subtracted. This yields $a = 1.76°C\ yr^{-1}$, $b = 1.22 \times 10^{-1}\ yr^{-1}$, $c = -1.47°C\ yr^{-1}$, and $d = 1.34 \times 10^{-2}°C\ yr^{-1}$. We have tested the dependence of the model RMS error on these coefficients, including the inversed damping time scale τ^{-1}. The strongest dependence is found for *a* and τ^{-1} as they control the long term GMST trend (Figure S5) and set the model transient climate sensitivity, which can be estimated for slow changes as $a \cdot \tau \log(2) \approx 2.4°C$ per CO_2 doubling.

Our simple model shares some similarities with the approach of *Thompson et al*. [2009], as both approaches consider relevant physical processes, but does differ in several important aspects. Specifically, their goal was to remove natural variability and extract anthropogenic effects on the evolution of GMST, but our study aims to reproduce the history of GMST since 1880 with a focus on the recent hiatus followed by a rapid temperature rise. Therefore, their approach was to remove temperature signals from each physical process separately and in several steps, using regressions, etc. Additionally, our model focuses on annual-mean values and thus neglects high-frequency variability induced, for example, by wintertime advection of marine air masses over continents in high latitudes as stressed in their study.

While highly idealized, our simple model reproduces the past GMST evolution very well (Figure 3a), with the RMS error over the instrumental record of about 0.08°C (Figure 3b). The model performs particularly well after the 1950s when more observations became available (RMS error ≈ 0.05°C). Furthermore, it captures the global warming hiatus and subsequent rapid temperature rise very accurately (Figure 3a), and the error for the past two decades reduces to 0.04°C (Figure 3b).

Systematic positive and negative errors are found for two time intervals, 1900–1930 and 1930–1960, respectively (Figure 3b), but we cannot rule out the possibility that they are caused by the poor data quality before the 1950s. For example, the fast cooling observed in the 1940s might be related in part to the discontinuity in the record noted by previous studies [*Thompson et al*., 2008]. Alternatively, the errors might arise because the global impacts of the Atlantic Multidecadal Oscillation (AMO) are not considered in our model, while these systematic errors coincide with the negative and positive phases of the AMO [*Enfield et al*., 2001].

5. Model Results: The Recent Hiatus and Subsequent Temperature Rise

Our next step is to use the simple model to understand the causes of the hiatus and the rapid resumption of GMST growth. Given the idealized setup of the model, we can isolate the impacts of different physical processes by suppressing individual forcings and integrating equation (1) with other model parameters fixed. When the ENSO forcing is suppressed, the modeled GMST exhibits a robust warming trend interrupted by substantial coolings associated with major volcanic eruptions (e.g., Mount Agung in 1963, El Chichón in

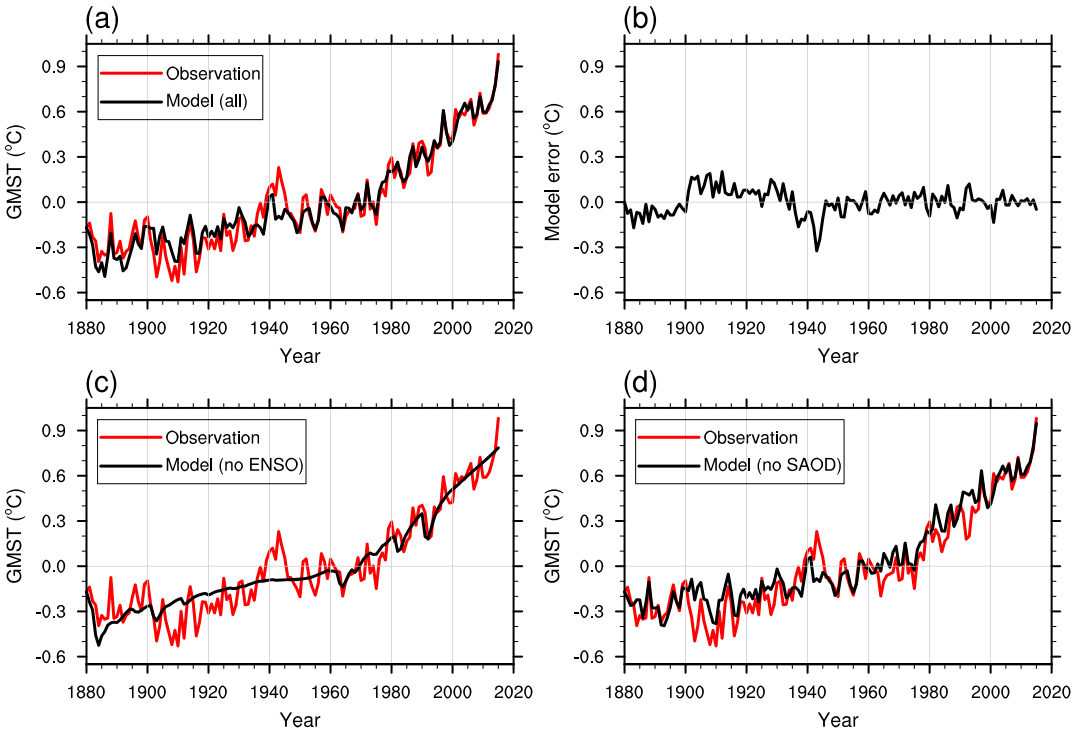

Figure 3. GMST variations estimated from the observations (red) and computed from the simple model (black). (a) All forcings are active, (c) ENSO forcing is suppressed, and (d) SAOD forcing due to volcanic eruptions is suppressed. (b) Model error, i.e., the difference between the model and the observations, for the scenario when all forcings are active (cf. Figure 3a). The error becomes smaller after 1950.

1982, and Pinatubo in 1991; Figure 3c). However, neither the global warming hiatus nor the rapid warming at the end of the record is reproduced. In contrast, when we turn the ENSO forcing back on but suppress the SAOD forcing, the two phenomena (the hiatus and the rapid warming) reappear, while discrepancies between the model results and the observations emerge during the years following volcanic eruptions (Figure 3d).

We can then calculate GMST trends during the hiatus period of 2001–2013 in different scenarios (Figure S6). When both ENSO and SAOD forcings are suppressed with CO_2 being the only active forcing, the modeled GMST trend during the hiatus period becomes 0.19°C/decade. The inclusion of ENSO forcing reduces the modeled GMST trend to 0.08°C/decade, close to the observed 0.05°C/decade, while the inclusion of SAOD forcing hardly affects the results. These conclusions hold regardless of the exact duration chosen for the hiatus period.

Accordingly, from our simple model, we do not find significant contributions of volcanic eruptions to the recent global warming hiatus as suggested by some studies [*Huber and Knutti*, 2014; *Santer et al.*, 2014]. Rather, our results indicate that ENSO-related anomalous heating originating in the tropical Pacific act to modulate GMST on interannual to interdecadal time scales, shaping the hiatus and the subsequent temperature increase. Model experiments using only ENSO forcing (CO_2 and volcanic eruptions suppressed) confirm that the cumulative effect of this forcing was positive in the 1980s and 1990s and negative after 2000, with decadal temperature variations reaching as large as 0.1°C (Figure 4), sufficient to mask the background global warming trend. At the same time, strong El Niño events lead to pronounced spikes in the simulated temperature record. Note, however, that due to the system's thermal inertia the spectrum of the ENSO-forced model temperature is "reddened" with respect to the original ENSO signal.

Our conclusions, drawn from an idealized simple model, are consistent with those of *Kosaka and Xie* [2016] who used comprehensive coupled simulations looking at the period before 2013. Our model, however, is more flexible for isolating physical processes and is much less expensive for conducting other tests.

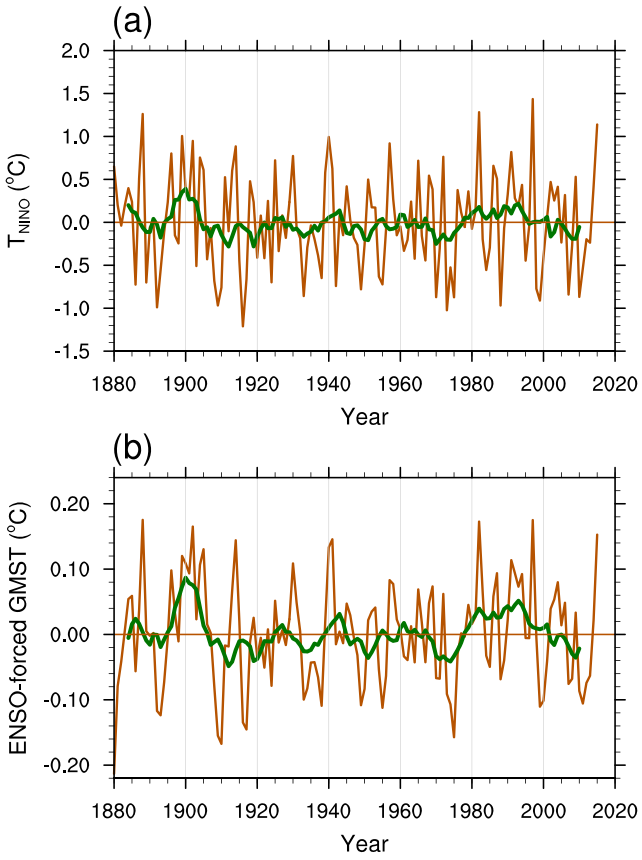

Figure 4. Variations in (a) equatorial SST index T_{NINO} and (b) model GMST when forced solely by this ENSO signal (with CO_2 and volcanic forcing suppressed). The brown lines indicate annual means, while the green lines indicate 10 year running means. Long-term means are removed from both variables. Note that the modeled GMST has less power at higher frequencies. This reddening is a consequence of the system's thermal inertia. The ENSO forcing generates decadal variations in GMST with amplitude of about ±0.05°C, which is sufficient to temporarily mask CO_2-induced trends of ~0.1°C per decade.

To further validate our results, we have adjusted the model coefficients by training the model by using observations only for 1880–1995, thus avoiding the usage of the most recent data that contains the hiatus. We then let the model make predictions for GMST during the next two decades with the input information on CO_2, ENSO, and SAOD. The best fit coefficients are now slightly different from those estimated for the full 1880–2015 records, but the model still successfully reproduces the hiatus and the temperature rise (Figure S7).

As we attribute the early 21st century global warming hiatus to weak El Niño activity since 2000, which followed strong warm events of the 1980s and 1990s,a question arises on the link of our results to previous studies that emphasized the role of the Pacific Decadal Oscillation or its broader defined equivalent the Interdecadal Pacific Oscillation (IPO) [e.g., *Kosaka and Xie*, 2013; *England et al.*, 2014; *Watanabe et al.*, 2014; *Dai et al.*, 2015]. We argue that our results are consistent with those studies as there is a strong connection between weak (strong) El Niño activity and the negative (positive) phase of IPO, even though whether these climate phenomena are closely related or simply influence one another remains under debate [see a recent review by *Newman et al.*, 2016].

Another warming hiatus that lasted from the mid-1940s to the 1970s and the subsequent accelerated warming has also drawn attention recently (Figure S6a) [e.g., *England et al.*, 2014; *Dai et al.*, 2015; *Zhang*, 2016; *Dong and McPhaden*, 2017]. Sensitivity tests with our simple model suggest that volcanic eruptions (mainly of the Mount Agung) and ENSO activity both played important roles in the 1946–1976 hiatus with the former being the primary factor (Figure S6b), consistent with previous studies [*Zhang*, 2016; *Dong and McPhaden*, 2017]. Note that the rate of CO_2 emission into the atmosphere was gradually rising over the last century, causing a significant increase in global warming trends with time. In fact, the CO_2-induced warming rate during the 1977–2000 period almost doubled relative to the preceding hiatus (Figure S6b).

Finally, we can use our simple model in combinations with ENSO seasonal forecasts to predict the next year GMST. Using July–June annual mean in this context is beneficial not only because El Niño typically peaks during boreal winter but also because ENSO forecasts are more reliable past the spring predictability barrier [*Torrence and Webster*, 1998; *McPhaden*, 2003]. Using the model parameters listed above and assuming weak La Niña conditions in 2016–2017 with a July–June mean equatorial cooling of about −0.2°C (e.g., NOAA Climate Prediction Center or European Centre for Medium-Range Weather Forecasts El Niño forecast), the model predicts a decrease of July–June mean GMST by 0.08°C with respect to the previous yearly interval,

which is far too small to affect the ongoing strong warming trend. Assuming neutral condition for this year would give only 0.05°C cooling of GMST.

6. Conclusion

In this study, we find that the equatorial Pacific tightly controls energy fluxes into the tropical atmosphere and thus modulates global mean surface temperature on interannual to interdecadal time scales. It is noteworthy that the equatorial Pacific, for example, the Niño region as defined in this study, occupies less than 3% of the globe; consequently, the typical annual-mean El Niño anomaly of about 0.7°C (Figure 2a) contributes only ~0.02°C to the GMST increase. This is an order of magnitude smaller than the observed GMST variations on interannual to interdecadal time scales, leaving atmospheric heating as the main mechanism by which tropical Pacific affects global mean temperature.

Motivated by these ideas, we have constructed a physically based model that utilizes the most essential climate information (CO_2 concentration, ENSO, and stratospheric aerosol optical depth) needed to reproduce the observed annual-mean GMST variations. Using the model results, we conclude that the global warming hiatus since 2000 was shaped primarily by ENSO variability and ended when the prolonged 2014–2016 El Niño conditions developed concurrently with the continuing global warming trend.

The simple model presented here has broad potential applications. For example, it can be used to diagnose the sensitivity of global climate models to individual forcings. It can also provide a metric for evaluating the performance of climate models from the perspectives of natural variability and externally forced climate response. Comparing the best fit model parameters for different climate states may shed light on the state dependence of transient climate sensitivity [*Caballero and Huber*, 2013]. Finally, when combined with proxies from ice cores, corals, or tree rings [*Cobb et al*., 2013; *Li et al*., 2013], the model can be applied to reconstruct past GMST history.

Acknowledgments
This research was supported by grants to A.V.F. from NOAA (NA14OAR4310277), NASA (NNX17AH21G), and NSF (AGS-1405272) and a NASA Earth and Space Sciences Graduate Fellowship to S.H. We also acknowledge computational support from the Yale University Faculty of Arts and Sciences High Performance Computing facility and from the NSF/NCAR Yellowstone Supercomputing Center. The data used in this study are available upon request from the authors (shineng.hu@yale.edu).

References

Caballero, R., and M. Huber (2013), State-dependent climate sensitivity in past warm climates and its implications for future climate projections, *Proc. Natl. Acad. Sci. U.S.A.*, *110*(35), 14,162–14,167.

Capotondi, A., et al. (2015), Understanding ENSO diversity, *Bull. Am. Meteorol. Soc.*, *96*(6), 921–938.

Cobb, K. M., N. Westphal, H. R. Sayani, J. T. Watson, E. Di Lorenzo, H. Cheng, R. L. Edwards, and C. D. Charles (2013), Highly variable El Niño–Southern Oscillation throughout the Holocene, *Science*, *339*(6115), 67–70.

Dai, A., J. C. Fyfe, S. P. Xie, and X. Dai (2015), Decadal modulation of global surface temperature by internal climate variability, *Nat. Clim. Change*, *5*(6), 555–559.

Deser, C., A. S. Phillips, R. A. Tomas, Y. M. Okumura, M. A. Alexander, A. Capotondi, J. D. Scott, Y. O. Kwon, and M. Ohba (2012), ENSO and Pacific decadal variability in the Community Climate System Model Version 4, *J. Clim.*, *25*(8), 2622–2651.

Dong, L., and M. J. McPhaden (2017), The role of external forcing and internal variability in regulating global mean surface temperatures on decadal timescales, *Environ. Res. Lett.*, *12*(3) 034011.

Enfield, D. B., A. M. Mestas-Nunez, and P. J. Trimble (2001), The Atlantic Multidecadal Oscillation and its relation to rainfall and river flows in the continental US, *Geophys. Res. Lett.*, *28*(10), 2077–2080, doi:10.1029/2000GL012745.

England, M. H., S. McGregor, P. Spence, G. A. Meehl, A. Timmermann, W. Cai, A. S. Gupta, M. J. McPhaden, A. Purich, and A. Santoso (2014), Recent intensification of wind-driven circulation in the Pacific and the ongoing warming hiatus, *Nat. Clim. Change*, *4*(3), 222–227.

Fedorov, A. V., S. Hu, M. Lengaigne, and E. Guilyardi (2015), The impact of westerly wind bursts and ocean initial state on the development, and diversity of El Niño events, *Clim. Dyn.*, *44*(5–6), 1381–1401.

Fyfe, J. C., et al. (2016), Making sense of the early-2000s warming slowdown, *Nat. Clim. Change*, *6*(3), 224–228.

Goddard Institute for Space Studies Surface Temperature Analysis Team (2017), GISS Surface Temperature Analysis (GISTEMP), NASA Goddard Institute for Space Studies. [Available at https://data.giss.nasa.gov/gistemp/. Dataset accessed 2016–09-10.]

Hansen, J., R. Ruedy, M. Sato, and K. Lo (2010), Global surface temperature change, *Rev. Geophys.*, *48*, RG4004, doi:10.1029/2010RG000345.

Hu, S., and A. V. Fedorov (2016), Exceptionally strong easterly wind burst stalling El Niño of 2014, *Proc. Natl. Acad. Sci. U.S.A.*, *113*(8), 2005–2010.

Hu, S., and A. V. Fedorov (2017), The extreme El Niño of 2015–2016: The role of westerly and easterly wind bursts, and preconditioning by the failed 2014 event, *Clim. Dyn.*, 1–19, doi:10.1007/s00382-017-3531-2.

Hu, S., A. V. Fedorov, M. Lengaigne, and E. Guilyardi (2014), The impact of westerly wind bursts on the diversity and predictability of El Niño events: An ocean energetics perspective, *Geophys. Res. Lett.*, *41*, 4654–4663, doi:10.1002/2014GL059573.

Huber, M., and R. Knutti (2014), Natural variability, radiative forcing and climate response in the recent hiatus reconciled, *Nat. Geosci.*, *7*(9), 651–656.

Kao, H. Y., and J. Y. Yu (2009), Contrasting Eastern-Pacific and Central-Pacific types of ENSO, *J. Clim.*, *22*(3), 615–632.

Karl, T. R., A. Arguez, B. Y. Huang, J. H. Lawrimore, J. R. McMahon, M. J. Menne, T. C. Peterson, R. S. Vose, and H. M. Zhang (2015), Possible artifacts of data biases in the recent global surface warming hiatus, *Science*, *348*(6242), 1469–1472.

Kaufmann, R. K., H. Kauppi, M. L. Mann, and J. H. Stock (2011), Reconciling anthropogenic climate change with observed temperature 1998–2008, *Proc. Natl. Acad. Sci. U.S.A.*, *108*, 11,790–11,793.

Kosaka, Y., and S. P. Xie (2013), Recent global-warming hiatus tied to equatorial Pacific surface cooling, *Nature*, *501*(7467), 403–407.

Kosaka, Y., and S. P. Xie (2016), The tropical Pacific as a key pacemaker of the variable rates of global warming, *Nat. Geosci.*, *9*(9), 669–673.

Kug, J. S., F.-F. Jin, and S.-I. An (2009), Two types of El Niño events: Cold tongue El Niño and warm pool El Niño, *J. Clim.*, *22*(6), 1499–1515.
Levine, A. F. Z., and M. J. McPhaden (2016), How the July 2014 easterly wind burst gave the 2015–2016 El Niño a head start, *Geophys. Res. Lett.*, *43*, 6503–6510, doi:10.1002/2016GL069204.
Levitus, S., et al. (2012), World ocean heat content and thermosteric sea level change (0–2000 m), 1955–2010, *Geophys. Res. Lett.*, *39*, L10603, doi:10.1029/2012GL051106.
Li, J. B., et al. (2013), El Niño modulations over the past seven centuries, *Nat. Clim. Change*, *3*(9), 822–826.
Liang, X. F., and L. Yu (2016), Variations of the global net air-sea heat flux during the "hiatus" period (2001–10), *J. Clim.*, *29*(10), 3647–3660.
Liu, W., S.-P. Xie, and J. Lu (2016), Tracking ocean heat uptake during the surface warming hiatus, *Nat. Commun.*, *7*, doi:10.1038/ncomms10926.
Lyman, J. M., S. A. Good, V. V. Gouretski, M. Ishii, G. C. Johnson, M. D. Palmer, D. M. Smith, and J. K. Willis (2010), Robust warming of the global upper ocean, *Nature*, *465*(7296), 334–337.
McPhaden, M. J. (2003), Tropical Pacific Ocean heat content variations and ENSO persistence barriers, *Geophys. Res. Lett.*, *30*(9), 1480, doi:10.1029/2003GL016872.
McPhaden, M. J. (2015), Commentary: Playing hide and seek with El Niño, *Nat. Clim. Change*, *5*(9), 791–795.
Menkes, C. E., M. Lengaigne, J. Vialard, M. Puy, P. Marchesiello, S. Cravatte, and G. Cambon (2014), About the role of westerly wind events in the possible development of an El Niño in 2014, *Geophys. Res. Lett.*, *41*, 6476–6483, doi:10.1002/2014GL061186.
Myhre, G., et al. (2013), Anthropogenic and natural radiative forcing, in *Climate Change 2013: The Physical Science Basis. Contribution of Working Group I to the Fifth Assessment Report of the Intergovernmental Panel on Climate Change*, edited by T. F. Stocker et al., pp. 659–740, Cambridge Univ. Press, Cambridge, U. K., and New York.
NASA News (2017), NASA, NOAA data show 2016 warmest year on record globally. [Available at https://www.nasa.gov/press-release/nasa-noaa-data-show-2016-warmest-year-on-record-globally. Accessed 2017–01-31.]
Neelin, J. D., F.-F. Jin, and H. H. Syu (2000), Variations in ENSO phase locking, *J. Clim.*, *13*(14), 2570–2590.
Newman, M., et al. (2016), The Pacific Decadal Oscillation, revisited, *J. Clim.*, *29*(12), 4399–4427.
Philander, S. G. H. (1990), *El Niño, La Niña and the Southern Oscillation*, Academic Press, New York.
Reynolds, R. W., T. M. Smith, C. Liu, D. B. Chelton, K. S. Casey, and M. G. Schlax (2007), Daily high-resolution-blended analyses for sea surface temperature, *J. Clim.*, *20*(22), 5473–5496.
Santer, B. D., et al. (2014), Volcanic contribution to decadal changes in tropospheric temperature, *Nat. Geosci.*, *7*(3), 185–189.
Sato, M., J. E. Hansen, M. P. Mccormick, and J. B. Pollack (1993), Stratospheric aerosol optical depths, 1850–1990, *J. Geophys. Res.*, *98*(D12), 22,987–22,994, doi:10.1029/93JD02553.
Schmidt, G. A., D. T. Shindell, and K. Tsigaridis (2014), Reconciling warming trends, *Nat. Geosci.*, *7*(3), 158–160.
Solomon, S., K. H. Rosenlof, R. W. Portmann, J. S. Daniel, S. M. Davis, T. J. Sanford, and G.-K. Plattner (2010), Contributions of stratospheric water vapor to decadal changes in the rate of global warming, *Science*, *327*, 1219–1223.
Solomon, S., J. S. Daniel, R. R. Neely III, J. P. Vernier, E. G. Dutton, and L. W. Thomason (2011), The persistently variable "background" stratospheric aerosol layer and global climate change, *Science*, *333*, 866–870.
Thompson, D. W. J., J. J. Kennedy, J. M. Wallace, and P. D. Jones (2008), A large discontinuity in the mid-twentieth century in observed global-mean surface temperature, *Nature*, *453*(7195), 646–649.
Thompson, D. W. J., J. M. Wallace, P. D. Jones, and J. J. Kennedy (2009), Identifying signatures of natural climate variability in time series of global-mean surface temperature: Methodology and insights, *J. Clim.*, *22*(22), 6120–6141.
Torrence, C., and P. J. Webster (1998), The annual cycle of persistence in the El Niño Southern Oscillation, *Q. J. R. Meteorol. Soc.*, *124*(550), 1985–2004.
Trenberth, K. E., J. M. Caron, D. P. Stepaniak, and S. Worley (2002), Evolution of El Niño-Southern Oscillation and global atmospheric surface temperatures, *J. Geophys. Res.*, *107*(D8), 4065, doi:10.1029/2000JD000298.
Watanabe, M., H. Shiogama, H. Tatebe, M. Hayashi, M. Ishii, and M. Kimoto (2014), Contribution of natural decadal variability to global warming acceleration and hiatus, *Nat. Clim. Change*, *4*(10), 893–897.
Xie, S.-P., Y. Kosaka, and Y. M. Okumura (2015), Distinct energy budgets for anthropogenic and natural changes during global warming hiatus, *Nat. Geosci.*, *9*, 29–33, doi:10.1038/ngeo2581.
Zhang, L. (2016), The roles of external forcing and natural variability in global warming hiatuses, *Clim. Dyn.*, *47*(9–10), 3157–3169.